Truncated Amyloid-(11-40/42) from Alzheimer Disease Binds Cu2+ with a Femtomolar Affinity and Influences Fiber Assembly.

Barritt, JD; Viles, JH

Truncated Amyloid-β(11-40/42) from Alzheimer's Disease Binds Copper^{2+} with a Femtomolar Affinity and Influences Fibre Assembly

Joseph D. Barritt, and John H. Viles

From the School of Biological and Chemical Sciences, Queen Mary, University of London, Mile End Road, London E1 4NS, UK

Running title: *Copper^{2+} binding to truncated amyloid-β*

To whom correspondence should be addressed:
Dr. John H. Viles, School of Biological and Chemical Sciences, Joseph Priestley Building, Queen Mary, University of London, Mile End Road, London E1 4NS, UK. Telephone: 44-020-7882-8443; E-mail: j.viles@qmul.ac.uk

Keywords: Cu^{2+}, Aβ, N-terminus, fibre kinetics, coordination

Background: N-terminally truncated $A\beta_{(11-40/42)}$ typically constitutes 19% of plaque load in Alzheimer's patients.

Results: Cu^{2+} binds to $A\beta_{(11-40)}$ with a 34 femtomolar dissociation constant and stabilizes very short highly amyloidogenic amyloid rods into longer Aβ fibres.

Concussion: The very tight affinity explains the high levels of Cu^{2+} in amyloid plaques.

Significance: Copper, tightly bound to $A\beta_{(11-40/42)}$ may influence disease pathology.

ABSTRACT

Alzheimer's disease (AD) coincides with the formation of extracellular amyloid plaques composed of the amyloid-β (Aβ) peptide. Aβ is typically forty residues long ($A\beta_{(1-40)}$) but can have variable C- and N-termini. Naturally occurring N-terminally truncated $A\beta_{(11-40/42)}$ is found in the cerebrospinal fluid and has a similar abundance to $A\beta_{(1-42)}$, constituting one fifth of the plaque load. Based on its specific N-terminal sequence we hypothesized that truncated $A\beta_{(11-40/42)}$ would have an elevated affinity for Cu^{2+}. Various spectroscopic techniques, complimented with transmission electron microscopy, were used to determine the properties of the $Cu^{2+}A\beta_{(11-40/42)}$ interaction and how Cu^{2+} influences amyloid fibre formation. We show $Cu^{2+}A\beta_{(11-40)}$ forms a tetragonal complex with a 34 ± 5 femtomolar dissociation constant at pH 7.4. This affinity is three orders of magnitude tighter than Cu^{2+} binding to $A\beta_{(1-40/42)}$ and more than an order of magnitude tighter than that of serum albumin, the extracellular Cu^{2+} transport protein. Furthermore, $A\beta_{(11-40/42)}$ forms fibres twice as fast as $A\beta_{(1-40)}$ with a very different morphology; forming bundles of very short amyloid rods. Substoichiometric Cu^{2+} drastically perturbs $A\beta_{(11-40/42)}$ assembly, stabilizing much longer fibres. The very tight femtomolar affinity of Cu^{2+} for $A\beta_{(11-40/42)}$ explains the high levels of Cu^{2+} observed in AD plaques.

The most prevalent form of fatal neurodegenerative disease is Alzheimer's disease (AD) which directly affects more than 30 million people worldwide (1). At the center of AD pathogenesis is the misfolding and self-assembly of an endogenous peptide, amyloid-beta (Aβ), into oligomers and amyloid fibres found in the extracellular plaques of AD patients (2). Aβ is released as a cleavage product of the amyloid precursor protein (APP) by the action of the β and

γ secretase complex, shown in Figure 1. These secretases, which have variable site specificity for APP, produce different lengths of Aβ, reviewed by Kummer and Heneka (3).

In addition to variable C-terminal cleavage, with Aβ reportedly being 39-43 residues in length (4,5). N-terminally truncated Aβ is also prominent in AD plaques. Exopeptidases such as aminopeptidase A are thought to be responsible for removing single residues from the N-terminus of the peptide (6-8). However the main N-truncated form of Aβ is generated by a secondary β-secretase activity (β') localized to the trans-Golgi network which produces an N-terminally truncated $Aβ_{(11-40/42)}$, see Figure 1 (9,10). $Aβ_{(11-40/42)}$ has also been identified as one of the main allotypes of Aβ in cerebrospinal fluid (CSF) (11).

It is perhaps not widely appreciated that isolated plaques from sporadic AD patients show $Aβ_{(11-42)}$ with a similar abundance to $Aβ_{(1-42)}$ with relative proportions of: $Aβ_{(1-40)}$ 45.8%; $Aβ_{(1-42)}$ 18.1% and $Aβ_{(11-42)}$ 18.6% (12). $Aβ_{(11-40/42)}$ and the N-terminal pyroglutamate allotype (pE $Aβ_{(11-40/42)}$) constitutes 19% of the relative Aβ load in the plaques of AD and young adults with Downs syndrome (13). Pyroglutamate (pE) at the N-terminal glutamate is generated by the action of the enzyme glutaminyl cyclase but the relative proportions of glutamate to pE are not well described (14). It is also thought that pE forms slowly over time, for example $Aβ_{(11-40/42)}$ detected in mouse models of AD contained no pyroglutamate, perhaps because these plaques form within 14 months (15). Interestingly, immunofluorescence has shown that pE $Aβ_{(11-40/42)}$ is concentrated at the core of plaques in AD brains; supporting the hypothesis that $Aβ_{(11-40/42)}$ could be one of the first amyloidogenic allotypes of Aβ to form plaques in AD (16). Furthermore mutations in presenilin-1 (PS1) linked with familial AD, increase levels of $Aβ_{(1-42)}$ but also, importantly $Aβ_{(11-42)}$ (17). Despite the prevalence of $Aβ_{(11-40/42)}$ in plaques and CSF, perhaps due to its poor solubility (18), very little is known about its amyloid forming properties *in vitro* or its synaptotoxicity.

There is considerable interest in the interaction of metal ions with Aβ (19). Cu^{2+} in particular, influences fibre formation and toxicity of $Aβ_{(1-40)}$ and $Aβ_{(1-42)}$ (19-24). The parenchymal copper concentration is at least four times higher in AD brains and Cu^{2+} is bound directly to Aβ in plaques (25-28). Changes in copper homeostasis exacerbate disease phenotype in rabbit and drosophila models of AD (29-31). Furthermore, sequestering copper with chelators such as clioquinol, or its derivatives, lowers Aβ aggregate load, maintains the health of AD mice and reduces toxicity in models of AD (32-34). Cu^{2+} is thought to bind to $Aβ_{(1-40/42)}$ with a 50-100 picomolar dissociation constant (35-37) and there is a suggestion that $Aβ_{(1-40/42)}$ may bind Cu^{2+} with a tighter affinity than this in an aggregated form (36). However, although the fluxes of weakly bound synaptic Cu^{2+} are thought to reach levels of 15-200 μM (38,39) it is still contested as to whether a 50 pM affinity is sufficient to retain Cu^{2+} ions in the brain parenchyma in the presence of other endogenous Cu^{2+} chelators. We wondered whether the concentration of Cu^{2+} in plaques might in part be due to Cu^{2+} binding to $Aβ_{(11-40/42)}$ with an even tighter affinity.

Interestingly, this truncated $Aβ_{(11-40/42)}$ contains a histidine (His_{13}) two amino acids from the N-terminal amino group. This bears a striking resemblance to the Cu^{2+} binding motif (NH_2-XxxXxxHis) at the N-terminus of human serum albumin (HSA) (40,41). This site is responsible for Cu^{2+} transport in blood plasma (42) and has a tight 1.0 picomolar affinity for Cu^{2+}, while N-terminal tripeptide models possess a sub-picomolar affinity (43-46).

Here we aim to characterize the amyloid forming properties of $Aβ_{(11-40)}$ and $Aβ_{(11-42)}$ and their interaction with Cu^{2+}. We show for the first time that $Aβ_{(11-40/42)}$ has heightened amyloidogenicity compared to $Aβ_{(1-40/42)}$ and forms short amyloid rod shaped assemblies. Furthermore, we show Cu^{2+} has an extremely tight, 34 ± 5 femtomolar dissociation constant for $Aβ_{(11-40)}$ at pH 7.4, and has a marked influence on $Aβ_{(11-40)}$ fibre formation and morphology. $Aβ_{(11-40/42)}$ constitutes 19% of the plaque load and this work suggests that it is responsible for the high concentration of Cu^{2+} found in the plaques of AD patients.

EXPERIMENTAL PROCEDURES

Aβ Peptides—Peptides used were synthesized using F-moc deprotection chemistry, including:

$A\beta_{(1-40)}$ DAEFR HDSGY EVHHQ KLVFF AEDVG SNKGA IIGLM VGGVV
$A\beta_{(11-40)}$ EVHHQ KLVFF AEDVG SNKGA IIGLM VGGVV
$A\beta_{(11-42)}$ EVHHQ KLVFF AEDVG SNKGA IIGLM VGGVV IA
These peptides, found in the CSF and plaques, include a free N-terminal amino group and C-terminal carboxylate. Pentapeptide models of the Cu^{2+} binding motif were C-terminally amidated to mimic the continuation of the peptide sequence in full length $A\beta_{(11-40/42)}$. The peptides were removed from the resin and deprotected before being purified by reverse-phase high-performance liquid chromatography. The samples were characterized using mass spectrometry. Peptides with amidated C-termini and free N-terminal amino groups studied included NH_2-EVHHQ-$CONH_2$ and NH_2-EVHAQ-$CONH_2$. Pentapeptides purchased from Generon Ltd. (Maidenhead, U.K.). Full length $A\beta_{(11-40)}$, $A\beta_{(11-42)}$ and $A\beta_{(1-40)}$ purchased from EZ Biolabs (Carmel, IN, USA) and Cambridge Research Biochemicals (Billingham, U.K.).

Aβ Solubilization—All three Aβ peptides, $A\beta_{(1-40)}$, $A\beta_{(11-40)}$ and $A\beta_{(11-42)}$ were solubilized at a concentration of 100 μM in water at pH 10.5 – 11, and then left at 4℃ for 48-72 hours. In our hands we found that this was the most effective solubilization method, as others have reported (47,48). It is clear that solubilized preparations of $A\beta_{(1-40)}$ and $A\beta_{(11-40)}$ are largely seed-free at pH 7.4 as solubilized preparations typically have no ThT fluorescence at time zero and exhibit a distinctive lag-phase of over 20 hours for $A\beta_{(11-40)}$ and 60 hours for $A\beta_{(1-40)}$. Freshly solubilized $A\beta_{(11-40)}$ and $A\beta_{(1-40)}$ peptides had no detectable assemblies under TEM. For $A\beta_{(1-40)}$, the concentration was determined using tyrosine absorption at 280 nm ε_{280} = 1,280 $cm^{-1}M^{-1}$. $A\beta_{(11-40)}$ and $A\beta_{(11-42)}$ lack a tyrosine residue so the peptide absorbance at 214 nm ε_{214} = 923 $cm^{-1}M^{-1}$ per amide was used (49). All lyophilized peptides typically contained 10 – 20 % moisture by weight. Concentrations for $A\beta_{(11-40/42)}$ were supported by the 1:1 saturation of the Cu^{2+} binding site, indicating that a very clear 1:1 stoichiometry had been established for freshly solubilized $A\beta_{(11-40/42)}$.

Titrations—All chemicals were purchased from Sigma-Aldrich at the highest purity available, and UHQ water was used throughout (resistivity of 10^{-18} Ω^{-1} cm^{-1}). Small aliquots of fresh aqueous stock solutions, typically 10 mM, were used to add metal ions ($CuCl_2 \cdot 2H_2O$, $NiCl_2 \cdot 6H_2O$) and competitive ligands, Glycine (500 mM) and L-Histidine (50 mM) stocks for titrations. Titrations were conducted at pH 7.4 with adjustments made using 20-100 mM solutions of NaOH and HCl. pH measurements were made before and after spectroscopic measurements.

Affinity Measurements—The conditional affinities at pH 7.4 were determined using glycine and L-histidine as competing ligands. The range of competitor concentrations (glycine and histidine) with Cu^{2+}:$A\beta_{(11-40)}$ or Cu^{2+}:$A\beta_{(11-15)}$ (0.8 : 1.0) complexes were made up in advance and left for 12 hours at pH 7.4 to ensure equilibrium had been reached. Repeat CD spectra were obtained over a few hours, to confirm equilibrium had been reached. The concentration of competitor required for equal molar equivalents of Cu^{2+} to be bound to both the Aβ peptide and competitor was used to determine the affinity of Cu^{2+} for the Aβ peptide using equation 1 (35,37,50). $Cu^{2+}{}_{free}$ is the concentration of Cu^{2+} not bound to either competitor ligand or peptide.

$$K_d = [Cu^{2+}{}_{free}] = \frac{[Cu^{2+}{}_{total}] - [Cu^{2+}{}_{bound\ to\ A\beta}]}{1 + K_{a1}[Gly_{free}] + K_{a1}K_{a2}([Gly_{free}]^2)}$$

Equation 1

At 50% saturation:

$$[Gly_{free}] = [Gly_{total}] - 2[Cu(Gly)_2] \qquad \text{Equation 2}$$

The Cu^{2+} affinities of each competitor at pH 7.4 can be calculated. K_{a1} and K_{a2} at pH 7.4 are: 7.4×10^5 M^{-1}, 7.4×10^4 M^{-1} for Gly and 2.7×10^8 M^{-1}, 2.1×10^6 M^{-1} for His (51).

Fibre growth assay—The kinetics of amyloid fibre formation were monitored using binding of Thioflavin T (ThT) to amyloid fibres, which induces ThT to fluoresce at 487 nm; this signal is

proportional to the amount of amyloid fibrils present (52). BMG-Galaxy and Omega FLUOstar fluorescence 96-well plate readers were used for the measuring of ThT fluorescence. Fluorescence readings were typically taken every 30 mins, following 30 seconds of gentle agitation. Fluorescence excitation and emission detection were obtained using filters at 440 nm and 490 nm respectively. Fibre growth kinetics are sensitive to a number of factors, including pH, concentration of Aβ, agitation, ionic strength and temperature; consequently, measures were taken to reduce variance in these parameters. All Aβ peptides were studied at 10 μM and all fibre growth experiments were incubated at 30℃ in 30 mM HEPES buffer (due to its low affinity for Cu^{2+} ions) and 160 mM NaCl. The pH, a critical factor in rate of fibre growth, was adjusted to pH 7.4 if necessary with small additions of 20-100 mM NaOH and HCl. Variation between samples was measured to be 0.05 pH units or less. 10 μM of ThT was present (1:1 with Aβ), which is optimal for tracking Aβ amyloid growth (52).

Growth curve analysis—Conversion of essentially monomeric Aβ to amyloid fibres follows a characteristic growth curve, consisting of an initial lag-phase (nucleation) before a growth phase (elongation). A growth curve can be fitted to the data, to obtain a number of empirical parameters, using the following equation (53):

$$y = (\upsilon_i + m_i x) + \frac{(\upsilon_f + m_f x)}{(1+e^{-\left(x-\frac{x_0}{\tau}\right)})}$$

Equation 3

y represents fluorescent intensity, and x represents time. Initial fluorescence intensity is represented by υ_i, υ_f represents the final fluorescence intensity, and x_0 is the time at which half maximal fluorescence is reached (t_{50}). The conditional fibre growth rate (k_{app}) is obtained by $1/\tau$ and the lag-time (t_{lag}) by $x_0 - 2\tau$. Data was processed using KaleidaGraph 4.0. Typically 6 or more kinetic traces were used to extract kinetic parameters.

Circular Dichroism (CD)—CD spectra were recorded at 25 °C on an Applied Photophysics Chirascan instrument between 250 and 700 nm, with sampling points every 2 nm, using a 1 cm path-length. Three repeat scans were made and baseline spectra were subtracted from each spectra, followed by smoothing using a 5 nm window, if required. Data were processed using Applied Photophysics Chirascan Viewer, Microsoft Excel, and KaleidaGraph spreadsheet/graph package. CD ellipticity measurements (θ, millidegrees), were converted to Δε (molar CD, M^{-1} cm^{-1}) using the relationship $\Delta\varepsilon = \theta/(33000.c.l)$, where c is the molar concentration and l is the path length. Note, molar ellipticity [θ] (degree cm^{-1} $dmol^{-1}$) = Δε 3300.

Transmission electron microscopy (TEM) —Aliquots of Aβ samples from the fibre growth assays were added to glow-discharged carbon-coated 300-mesh copper grids (Structure Probe, Inc. West Chester, USA.) using the droplet method, with water washes before and after addition of stain. Phosphotungstic acid (PTA) (2 % w/v), adjusted to pH 7.4, was used to negatively stain the assemblies. PTA was prepared and incubated at 37℃ for 24-48 hours prior to filtering immediately before use. Selected images are representative of multiple images that were taken over a number of fields and grids. Images were recorded using a JEOL JEM-1230 electron microscope operated at 80 kV, and the Olympus iTEM software package.

Electron Paramagnetic Resonance (EPR) —EPR was carried out on a Bruker Elexsys E580 spectrometer at an X-band (9.38 GHz) microwave frequency at 0.5 mW. Single scans were made in EPR quartz tubes (outside diameter 4 mm, inside diameter 3 mm) with a 2000 G sweep width centered at 3000 G and a 10 G modulation amplitude. 50 mM of 60% HEPES/40% phosphate buffer was used at pH 7.4 for temperature-independent buffering at 10 K temperatures.

^{1}H-NMR—^{1}H-NMR spectra were recorded on a Bruker AV600 spectrometer Using 500 μM of EVHHQ peptide in 100% D_2O, 30 mM phosphate buffer at pH* 7.4. $CuCl_2$ aliquots were added from 10 mM. stocks of $CuCl_2 \cdot 2H_2O$ in 100% D_2O. Data was processed and analyzed using TopSpin 2.1 (Bruker) software.

RESULTS

Aβ$_{(11-40)}$ and Aβ$_{(11-42)}$ rapidly forms amyloid rods— Although N-terminally truncated Aβ$_{(11-40)}$ and Aβ$_{(11-42)}$ constitute 20% of AD plaque load, very little is known about their ability to form amyloid fibres. We therefore monitored the kinetics of Aβ$_{(11-40)}$ and Aβ$_{(11-42)}$ fibre formation using the amyloid specific fluorescent dye, thioflavin T (ThT). After solubilization at high pH, Aβ$_{(11-40)}$ was diluted to 10 μM at pH 7.4 and ThT fluorescence was monitored over time in a 96-well-plate reader. The kinetics of Aβ$_{(11-40)}$ fibre formation were compared to Aβ$_{(1-40)}$. Like Aβ$_{(1-40)}$ a sigmoidal fibre growth curve was consistently observed for Aβ$_{(11-40)}$ with a clear nucleation and elongation phase, shown in Figure 2a. Aβ$_{(11-40)}$ forms fibres significantly faster than Aβ$_{(1-40)}$, with an accelerated nucleation and elongation rate. Under the same conditions Aβ$_{(11-40)}$ has a nucleation time of 27 ± 0.3 hours compared to 65 ± 1 hours for Aβ$_{(1-40)}$. The elongation rates for Aβ$_{(11-40)}$ and Aβ$_{(1-40)}$ are 0.44 ± 0.02 hour^{-1} and 0.23 ± 0.04 hour^{-1} respectively. Total maximal ThT fluorescence for the two Aβ forms are similar at 10 μM, suggesting both form comparable amounts of amyloid, detectable by ThT.

Next we wanted to investigate the types of Aβ assemblies generated. Transmission electron microscopy (TEM) of Aβ$_{(11-40)}$, shown in Figure 2b, consistently revealed stacking of straight, very short rod-shaped fibres. Only short, stacked rods were observed across multiple peptide batches, solubilizations and TEM grids. The rods have a similar thickness (*ca.* 10 nm) to Aβ$_{(1-40)}$ fibres (Fig. 2c) but are much shorter with the majority being under 50 nm in length. These amyloid rods do not extend beyond 500 nm, as shown in Figure 2d. Furthermore, individual fibre rods tend to self-associate into clumps much more readily than that of the typically long, twisted Aβ$_{(1-40)}$ fibres, shown in Figure 2c, formed on the same well-plate under the same conditions.

Aβ$_{(11-42)}$ was also solubilized at high pH with the method used for Aβ$_{(11-40)}$. The ThT fluorescence of Aβ$_{(11-42)}$ produced a sigmoidal growth curve with a nucleation and elongation phase. Under the same conditions, both Aβ$_{(11-40)}$ and Aβ$_{(11-42)}$ have quite a similar nucleation phase with lag times of 27 ± 0.3 hours and 25 ± 1 hours respectively, shown in Figure 2a. Aβ$_{(11-42)}$ has some fluorescence signal directly after solubilization, suggesting some amyloid assemblies persist even after solubilization.

TEM images revealed some different morphological features for Aβ$_{(11-42)}$ compared with Aβ$_{(11-40)}$. Aβ$_{(11-42)}$ contains short stacked rods just like Aβ$_{(11-40)}$, figure 2e, but there are also longer twisted fibres, figure 2f, often with ragged oligomeric assemblies along the length of the fibre. Also present are some highly stained disordered amorphous aggregates which are in greater abundance in Aβ$_{(11-42)}$ than Aβ$_{(11-40)}$ images. We were interested in why Aβ$_{(11-40)}$ formed much shorter fibre rods. We wondered if Aβ$_{(11-40)}$ rods were caused by fibre fragmentation so we generated Aβ$_{(11-40)}$ fibres in the absence of the mild agitation used in the previous experiment. Quiescently generated fibres show a clear change in the fibre length of Aβ$_{(11-40)}$. Although numerous short amyloid-rods were present, much longer fibres, (which were not observed under mild agitation conditions) were also observed, figure 3a. This suggests that Aβ$_{(11-40)}$ forms exclusively short amyloid rods because it readily fragments. The differences in quiescently generated Aβ$_{(11-42)}$ fibres were less marked but the short rods were less abundant with a greater relative abundance of longer fibres, figure 3b

Cu^{2+} tetragonal coordination to Aβ$_{(11-40)}$—There is a well-established link between Cu^{2+} homeostasis and AD; we therefore wanted to investigate the Cu^{2+} binding properties of Aβ$_{(11-40/42)}$. For this we have used visible CD and EPR spectroscopy. When bound to proteins and peptides Cu^{2+} can produce very characteristic d-d vis-CD bands (54,55). Cu^{2+} derived vis-CD bands arise from amide-main chain coordination being in close proximity to the chiral center, fixed in a chelate ring (56,57). Figure 4a shows an overlay of the vis-CD spectra of the N-terminal residues for Aβ$_{(11-40)}$ and a more soluble N-terminal pentapeptide Aβ$_{(11-15)}$ (NH_2-EVHHQ-Am) with 1:1 molar equivalents of Cu^{2+}. The spectra are almost identical, suggesting that only the first few N-

terminal residues of $A\beta_{(11-40)}$ are involved in coordinating Cu^{2+} ions.

In light of the possible similarity between Cu^{2+} binding at the N-terminus of human serum albumin (HSA) and $A\beta_{(11-40)}$ (in particular, both contain the NH_2-XxxXxxHis Cu^{2+} binding motif) we directly compared the vis-CD spectra of Cu^{2+} loaded $A\beta_{(11-40)}$ with that of HSA and two albumin peptide models: NH_2-AspAlaHis-Am and NH_2-AlaAlaHis-Am. It is clear from Figure 4b that the Vis-CD spectra are very similar. There are some minor differences in the relative intensity of the positive and negative CD bands but in comparison to the wavelength shifts seen between HSA and its N-terminal peptide models, these are not significant enough to suggest a different binding conformation (58).

The stoichiometry of the Cu^{2+} $A\beta_{(11-40)}$ interaction was investigated though a $CuCl_2$ titration monitored by vis-CD with $A\beta_{(11-40)}$ and $A\beta_{(11-15)}$, shown in Figure 4c. The CD band intensity increases with the addition of Cu^{2+} up to 1 molar equivalent, indicating a 1:1 stoichiometry. A single set of CD bands are observed throughout the titration, suggesting a single complex is formed even at low, substoichiometric amounts of Cu^{2+}. The Cu^{2+} complex is stable over a large physiological pH range; with a mid-point for the complex of 4.7, at the transition between the CD active Cu^{2+} complex and no CD signal. Figure 4d shows the pH dependence of the $Cu^{2+}A\beta_{(11-15)}$ complex. There is no change in the wavelength position of the CD bands; indicating that a single CD active complex is formed between pH 5.5 and 10. It is clear the same Cu^{2+} complex forms over a large range of pH values.

Electron paramagnetic resonance (EPR) was also used to study the coordination geometry of the $Cu^{2+}A\beta_{(11-15)}$ complex. The Cu^{2+} loaded EPR spectra exhibited Cu^{2+} type-II spectra typical of a square-planar/tetragonal coordination geometry, shown in Figure 5a. Furthermore the g_{II} of 2.17 and hyperfine splitting, A_{II} of 19.3 mK, is most indicative of four nitrogen coordinating ligands (59). The $Cu^{2+}A\beta_{(11-15)}$ EPR spectra bares a close resemblance to the EPR spectra of albumin's N-terminal Cu^{2+} binding site, also shown in Figure 5a. The g_{II} and A_{II} values are very similar, further supporting that the $Cu^{2+}A\beta_{(11-15)}$ complex has a square-planar, four nitrogen coordination similar to that found for albumin, with the N-terminal amino group, the next two amide main-chain nitrogens and the imidazole ring nitrogen coordinating, as shown in Figure 5b.

We were interested in investigating if Cu^{2+} would bind to the amyloid fibril rods of $A\beta_{(11-40)}$ in a similar manner to the monomer. Using vis-CD we show that Cu^{2+} was able to bind to preformed $A\beta_{(11-40)}$ fibre rods. The vis-CD spectra bears a close resemblance to the Cu^{2+} $A\beta_{(11-40)}$ monomer complex with comparable wavelengths and intensity of vis-CD bands, as shown in Figure 6. Fibrillar Cu^{2+} $A\beta_{(11-40)}$ exhibits 0.7:1 binding stoichiometry, close to 1:1. This suggests the Cu^{2+} binding complex within the first three residues at the N-terminus is accommodated within the amyloid fibre structure. We note, from this binding curve a 0.5:1 stoichiometry, although unlikely, cannot be ruled out in fibres.

Femtomolar Cu^{2+} conditional dissociation constant for $A\beta_{(11-40)}$—The affinity of Cu^{2+} binding to $A\beta_{(11-40)}$ and its more soluble peptide model $A\beta_{(11-15)}$ was determined using a number of competitive ligands with known affinities for Cu^{2+}. The tight affinity of Cu^{2+} for $A\beta_{(11-40)}$ requires a highly soluble competitor so glycine and histidine were chosen for their relatively high solubility. Glycine has a micromolar affinity for Cu^{2+} and forms a bidentate complex via its amino and carboxylate groups. While histidine has a nanomolar affinity and can coordinate Cu^{2+}, forming a $Cu^{2+}(His)_2$ bidentate complex at physiological pH (60).

The $Cu^{2+}(Gly)_2$ complex is CD silent so the vis-CD signal for Cu^{2+}:$A\beta_{(11-15)}$ can readily be used to determine affinity. A very large excess of glycine is needed to compete with 100 μM of $A\beta_{(11-15)}$ to bind Cu^{2+}; as much as 3,000 molar equivalents of glycine (170 mM) is required to remove half of the Cu^{2+} from $A\beta_{(11-15)}$, shown in Figure 7a. Histidine has a tighter nanomolar affinity for Cu^{2+} but it still requires 50 molar equivalents (1.4 mM) to remove half the Cu^{2+} ions from $A\beta_{(11-15)}$, Figure 7b. Strikingly, it takes more than 100 molar equivalents of histidine to compete all of the Cu^{2+} from $A\beta_{(11-15)}$. At this point the $Cu^{2+}(His)_2$ vis-CD spectrum becomes apparent with characteristic weak positive CD bands at 270 nm and 780 nm.

The concentration of competing ligand required to remove half of the Cu^{2+} from $A\beta_{(11-15)}$ can be used to determine the affinity using equation 1, see experimental. The molar ellipticity from the vis-CD spectra bands at 276 nm, 316 nm, 480 nm and 558 nm are used to gain an insight into the errors in fitting the binding curves. In addition, the titrations were repeated for each competitive ligand. Table I shows affinities determined with histidine and glycine. Using glycine as a competitor, a K_d of 2.5 x 10^{-14} M was determined at pH 7.4. While for histidine a K_d of 4.2 x 10^{-14} M was calculated. An ANOVA shows there is no significant difference in the values determined using histidine and glycine as competitors with a P value of 0.20 across the four titrations. It is clear that the conditional dissociation constant at pH 7.4 of Cu^{2+} for $A\beta_{(11-15)}$ is in the femtomolar range with a mean K_d of 34 ± 5 fM determined. The agreement in affinity determined using two different competing ligands, indicates the measurements are not complicated by the formation of a ternary complex between Cu^{2+}, $A\beta_{(11-15)}$ and competitor.

A similar glycine competition titration of the full-length monomeric Cu^{2+} $A\beta_{(11-40)}$ complex was performed, shown in Figure 7c. A similar K_d of 10 ± 3 fM was measured. This data is less reliable as $A\beta_{(11-40)}$ is less soluble and there is some light scatter in the data which affects the vis-CD signal, however it is clear $A\beta_{(11-40)}$ binds to Cu^{2+} with an affinity of 34 fM or tighter.

Evidence for square-pyramidal His_{14} coordination of Cu^{2+} —The affinities determined for $A\beta_{(11-40)}$, in Table I, are tighter than those reported for human serum albumin and we considered the possibility that the higher affinity might be due to the presence of a second histidine residue, His_{14}, four residues from the N-terminus. To investigate this we generated a peptide analogue with an alanine substitution at the His_{14} site. Using competing ligands we determined the affinity of Cu^{2+} for $A\beta_{(11-15)}$ His_{14}Ala. In this way we have determined if His_{14} has an influence on the Cu^{2+} affinity. The dissociation constant at pH 7.4, determined using glycine or histidine as competing ligands, was 136 ± 23 fM. This value is slightly weaker than the complex with His_{14} present, with a P value of < 0.05 showing a significant difference between His_{14} and alanine substituted $A\beta_{(11-15)}$ affinities. Based on the K_d data it does appear His_{14} has an influence on the affinity of Cu^{2+} for $A\beta_{(11-40)}$.

The Cu^{2+} vis-CD and UV-vis absorption spectra of $A\beta_{(11-15)}$ are very similar compared to the His_{14}Ala analogue, with a high degree of similarity between the vis-CD band wavelengths and intensities. In addition, the visible absorption spectra for Cu^{2+} $A\beta_{(11-15)}$ and $A\beta_{(11-15)}$ His_{14}Ala, are very similar. A λ_{max} at 525 nm and a molar extinction coefficient ε_{525} of 110 $M^{-1}cm^{-1}$ for both peptides are indicative of other NH_2-XxxXxxHis Cu^{2+} complexes (45). This further supports the formation of a characteristic NH_2-XxxXxxHis Cu^{2+} complex similar to that of the N-terminal Cu^{2+} binding site of albumin.

We wanted to use ^{1}H-NMR to help further resolve this question. Addition of paramagnetic Cu^{2+} causes a loss of $A\beta_{(11-15)}$ ^{1}H NMR signal intensity with increasing additions of Cu^{2+}. Cu^{2+} bound ^{1}H NMR signals are not observed due to the paramagnetic properties of Cu^{2+}, which cause significant line-broadening of ^{1}H-NMR signals. There is no difference in the extent to which signal is lost between His_{13} and His_{14} resonances as Cu^{2+} is added, which is consistent with a role for His_{14} in axial coordination. However this could be due to the proximity of His_{14} ring protons to Cu^{2+} rather than direct coordination, as all the side-chain resonances are extensively broadened.

Cu^{2+} and $A\beta_{(11-40)}$ fibre formation—We have shown $A\beta_{(11-40)}$ has an appreciable femtomolar affinity for Cu^{2+}, we therefore wanted to investigate how the presence of Cu^{2+} ions might affect the kinetics and morphology of $A\beta_{(11-40)}$ fibre formation. ThT fluorescence indicates that the presence of 0.1 molar equivalents of Cu^{2+} has little effects on fibre kinetics, while 0.2 molar equivalents causes a reduction in the total ThT signal by approximately 40%, see figure 8a. A similar ThT signal reduction is observed with 0.4 molar equivalents of Cu^{2+} but there is a prominent reduction in elongation rate, with k_{app} slowing from 0.54 ± 0.02 $hours^{-1}$ for apo to 0.21 ± 0.04 $hours^{-1}$. For 1 and 10 molar equivalents of Cu^{2+}, no ThT signal is observed over more than 100 hrs. Interestingly, not only do small substoichiometric

amounts of Cu^{2+} perturb the kinetics of $A\beta_{(11-40)}$ fibre formation, and the total amount of ThT bound to amyloid, but Cu^{2+} also affects the morphology of the fibres generated. In the absence of Cu^{2+}, $A\beta_{(11-40)}$ exclusively generates short amyloid rods (mostly 50 - 200 nm in length) under mildly agitating conditions, as shown in Figure 2. However, with fibres generated under the same mild agitation, the TEM images show that short rods only partially remain; even in the presence of small substoichiometric concentrations of 0.2 equivalents of Cu^{2+}. However, there are also similar amounts of much longer, twisted fibres with a morphology more reminiscent of $A\beta_{(1-40)}$, shown in Figure 8b. At just 0.4 equivalents Cu^{2+}, EM grids contain almost exclusively long fibrillar assemblies. Counter intuitively, although at 0.4 molar equivalents of Cu^{2+} the ThT signal is attenuated, the EM images show numerous and wide-spread long amyloid fibres, Figure 8c, but there is an increased amount of amorphous aggregates compared to lower Cu^{2+} equivalents. Beyond 1 molar equivalent of Cu^{2+} the TEM images are dominated by amorphous aggregates with dense irregular staining of the aggregates, not shown, which do not cause ThT fluorescence.

We were also interested in discovering if the long fibres generated in the presence of Cu^{2+} revert to short rods in the presence of a strong Cu^{2+} chelator, for this experiment we added Ethylenediaminetetraacetic acid (EDTA) which has a K_a of 10^{18} for Cu^{2+}. The addition of EDTA to $A\beta_{(11-40)}$ fibres, generated in the presence of 0.4 molar equivalents Cu^{2+}, caused the ThT fluorescence signal to increase to a similar intensity to that observed for apo $A\beta_{(11-40)}$, as shown in Figure 9a, thus any reduction in ThT bound fibres is rapidly reversible. Interestingly TEM images of these $A\beta_{(11-40)}$ fibres grown with Cu^{2+} revert to very short stacks of amyloid rods, like those seen for fibres of $A\beta_{(11-40)}$ only. This observation suggests that Cu^{2+} has a stabilizing effect on $A\beta_{(11-40)}$ fibres, preventing fragmentation, but once Cu^{2+} is removed, all the fibres rapidly fragment into amyloid rods, as shown in Figure 9b.

Next we wanted to see if Cu^{2+} addition affects the morphology of preformed $A\beta_{(11-40)}$ amyloid rods as well. We know from Figure 6 that Cu^{2+} can bind to preformed amyloid fibres. Addition of Cu^{2+} to preformed amyloid rods of $A\beta_{(11-40)}$ caused a 32% reduction in ThT fluorescence. This reduced the intensity of fluorescence to a similar level to the maximum fluorescence observed for $A\beta_{(11-40)}$ fibres grown in the presence of 0.4 molar equivalents of Cu^{2+}. TEM images, shown in Figure 9c, demonstrate that addition of Cu^{2+} to the preformed, fragmented amyloid rods had no discernible effect over a 70 hour period.

Cu^{2+} and $A\beta_{(11-42)}$ fibre formation—We have recently shown, the effect of Cu^{2+} on fibre growth can markedly vary depending on the isotype of Aβ present (24). In particular, substoichiometric Cu^{2+} causes $A\beta_{(1-40)}$ to form fibres but with $A\beta_{(1-42)}$ only protofibrils and oligomers are observed. We therefore wanted to investigate the effect of Cu^{2+} on $A\beta_{(11-42)}$ fibre growth to assess how the two C-terminal amino acids influence Cu^{2+} dependent kinetics. As with $A\beta_{(11-40)}$, increasing the molar equivalents of Cu^{2+} causes the maximum ThT signal of each $A\beta_{(11-42)}$ fibre growth curve to decrease. The ThT signal reduction caused by 0.4 molar equivalents of Cu^{2+} is similar to $A\beta_{(11-40)}$, with a reduction for $A\beta_{(11-42)}$ of *ca.* 50%. The effect of Cu^{2+} on $A\beta_{(11-42)}$ elongation rate was similar to $A\beta_{(11-40)}$ with a slower rate with increasing Cu^{2+} levels.

The representative TEM images of $A\beta_{(11-42)}$ nucleated with Cu^{2+}, shown in Figure 8e and 8f, complimented the decrease in ThT fluorescence observed as $A\beta_{(11-42)}$ was grown with higher equivalencies of Cu^{2+}. There was a general decrease in short amyloid rod stacks while longer fibres were more abundant as more Cu^{2+} was added. There were also shorter, "curvy" assemblies with a morphology often observed for protofibrillar assemblies at 0.4 molar equivalents Cu^{2+}. The promotion of $A\beta_{(11-42)}$ protofibril generation by Cu^{2+} is similar to the effect observed for Cu^{2+} with $A\beta_{(1-42)}$ but the effect was by no means as universal as it is for $A\beta_{(1-42)}$ (24).

DISCUSSION

$A\beta_{(11-40/42)}$ rapidly forms amyloid rods—Appreciable levels of $A\beta_{(11-40/42)}$ are present in the CSF, produced by the action of BACE at the β' cleavage site of APP (10,11). Furthermore mean levels of Aβ within plaques from sporadic AD

patients have been shown to contain 19% $A\beta_{(11-42)}$, comparable to $A\beta_{(1-42)}$ levels (12,13). Despite this, perhaps because of its poor solubility (18), very few *in vitro* studies of $A\beta_{(11-40/42)}$ have been reported, with studies focusing almost exclusively on $A\beta_{(1-40/42)}$. This is the first study describing the kinetics of $A\beta_{(11-40/42)}$ fibre formation and its interaction with Cu^{2+} ions.

Under the same conditions (10 μM Aβ, pH 7.4, mild agitation) both $A\beta_{(11-40)}$ and $A\beta_{(11-42)}$ form ThT binding amyloid assemblies more than twice as fast as $A\beta_{(1-40)}$. Thus the rapid formation of amyloid rods of $A\beta_{(11-40/42)}$, that we observe, may be important in plaque deposition. The amyloidogenicity of Aβ sequences are often thought to correlate with disease progression. $A\beta_{(1-42)}$ forms fibres much faster than $A\beta_{(1-40)}$ and is also more toxic *in vivo* (61-64). The heightened rate of fibre nucleation and elongation observed for $A\beta_{(11-40/42)}$ may be caused by the loss of negatively charged side-chains as it is known that the pI and charge of Aβ have a profound influence on its rate of fibre formation (22,65). The absence of a number of charged residues at the N-terminus increases the theoretical pI from 5.1 for $A\beta_{(1-40/42)}$ to 6.0 for $A\beta_{(11-40/42)}$. Consequently, at physiological pH 7.4, $A\beta_{(11-40)}$ is more neutrally charged and will much more readily self-associate into nucleating oligomers and elongate more rapidly into fibres. $A\beta_{(11-40)}$ fibres generated quiescently form much longer fibres indicating $A\beta_{(11-40)}$ fibres fragment more easily than $A\beta_{(1-40)}$. It is known that secondary nucleation events can dominate the kinetics of fibre formation and influence cytotoxicity (66,67). The rapid fibre formation for $A\beta_{(11-40)}$ might be due, impart to its propensity to fragment and cause secondary nucleation.

We were interested by the markedly shorter rod-like fibres observed for apo $A\beta_{(11-40)}$ and $A\beta_{(11-42)}$ compared to $A\beta_{(1-40)}$. With the exception of the Aβ Osaka mutant (AβΔ22) (68), the first ten residues of $A\beta_{(1-40/42)}$ have been shown not to typically be directly involved in the core structure of most amyloid fibres generated *in vitro*, and are not thought to form any stable hydrogen bonded structure (69-71), despite this our data shows these residues have a profound influence on the appearance (length) of the fibres. It is possible that the N-terminal residues (1-10) have a stabilizing influence on the amyloid fibres as they form. $A\beta_{(11-42)}$ also forms largely short amyloid rods under mildly agitating conditions, although longer fibres are present, the two additional C-terminal residues could possibly stabilize the intermolecular forces along the fibre.

Cu^{2+} and $A\beta_{(11-40/42)}$—The presence of the histidine three residues from the N-terminus facilitates the formation of a high affinity Cu^{2+} complex. $A\beta_{(11-40)}$ and the model peptide $A\beta_{(11-15)}$ have a 34 ± 5 fM conditional dissociation constant for Cu^{2+} at pH 7.4. This indicates $A\beta_{(11-40/42)}$ binds to Cu^{2+} with a thousand times tighter affinity compared to $A\beta_{(1-40/42)}$ (35). It is clear that $A\beta_{(11-40/42)}$ will preferentially bind any available extracellular Cu^{2+} ions. Indeed $A\beta_{(11-40)}$ has an affinity more than an order of magnitude tighter than the extracellular Cu^{2+} transport protein human serum albumin (HSA). This has ramifications for the ability of $A\beta_{(11-40/42)}$ to compete for Cu^{2+} ions at the synapse. Cu^{2+} is released at the synapse during neuronal depolarization and is thought to reach levels between 15 and 200 μM (38). CSF levels of Cu^{2+} are lower, at 500 nM, (72) but the femtomolar affinity of $A\beta_{(11-40/42)}$ will readily bind Cu^{2+} even at these lower concentrations. The total soluble Aβ concentration in the CSF is 0.1 – 0.5 nM (11), so with such a high affinity for Cu^{2+} much of the $A\beta_{(11-40/42)}$ is likely to be coordinating Cu^{2+} ions. It is notable that the most abundant protein in the CSF, the Cu^{2+} transport protein serum albumin, reaches levels of 3 μM but has an affinity for Cu^{2+} more than an order of magnitude weaker than $A\beta_{(11-40/42)}$ and will therefore only partially compete for Cu^{2+} ions bound to $A\beta_{(11-40/42)}$. $A\beta_{(11-40/42)}$ can constitute up to 19% of the plaque load (12), and its presence can explain the very high levels of Cu^{2+} found in the plaques of AD patients (25-28).

The visible absorbance, vis-CD, EPR spectra, pH dependence, stoichiometry and NMR data are all initially consistent with the formation of a 4N, N-terminal complex shown in Figure 5b. We considered the possibility of the involvement of the imidazole nitrogen of His_{14} coordinating axially, perpendicular to the 4N plane. There is little difference in the absorbance spectra or

visible CD between the $A\beta_{(11-15)}$ model peptide and $A\beta_{(11-15)}$ H14A, which might suggest His_{14} is not involved in coordination, however axial coordination can have minimal influence on absorbance spectra for Cu^{2+} square-pyramidal complexes. There is a significant loss of affinity with the removal of the second histidine which suggests that His_{14} has an influence on coordination, forming a square pyramidal complex with axial coordination from the imidazole of His_{14}, making the affinity of $A\beta_{(11-40/42)}$ considerably tighter than that observed for serum albumin (HSA) at 1.0 pM (46).

The vis-CD spectra generated for Cu^{2+} $A\beta_{(11-40)}$ monomers and fibres are almost identical, indicating that Cu^{2+} binds to fibres with a similar coordination to that of the monomer. Vis-CD spectra are extremely sensitive to coordination; the intensity and even sign of the CD bands will be greatly influenced by even small changes in geometry (57,58). Cu^{2+} cross-linking between two adjacent Aβ molecules is not supported by the data. In particular, the loss of main-chain amide coordination to be replaced by side-chain coordination from a histidine imidazole of a second Aβ molecule is likely to cause a profound change in the appearance of the CD bands, which is not observed. The ability of amyloid fibres to accommodate Cu^{2+} binding has also been observed for $A\beta_{(1-40)}$ and $A\beta_{(1-42)}$ (35,73-76). Interestingly, Cu^{2+} can diffuse into and load on to all Aβ molecules within the fibres and facilitate the Cu^{2+} coordination with close to 1:1 stoichiometry.

It is not clear why the presence of Cu^{2+} would promote markedly longer fibres compared to the much shorter, rod-like fibres observed for apo $A\beta_{(11-40)}$, generated under the same conditions of mild agitation. The binding of Cu^{2+} ions appears to stabilize longer fibres that would otherwise fragment into shorter rods. This is supported by the effect of EDTA addition to Cu^{2+} $A\beta_{(11-40)}$ fibres which results in rapid fragmentation of $A\beta_{(11-40)}$ into shorter amyloid rods. The molecular packing of $A\beta_{(11-40)}$ fibres in the presence of Cu^{2+} seems to produce a greater fibre stability against shearing forces that cause fragmentation (66). We suggest that at pH 7.4, the addition of Cu^{2+} will add positive charge to $A\beta_{(11-40)}$, and with a pI of 6.0 $A\beta_{(11-40)}$ may be closer to charge neutrality which might stabilize fibres. Potentially the Cu^{2+} complex could cross-link between the His_{13} and His_{14} residues of two adjacent Aβ molecules within a fibre, stabilizing the extension of the fibre resulting in longer structures, however there is no evidence for a change in coordination geometry for $A\beta_{(11-40)}$ monomer or fibres, so this seems unlikely.

The marked influence of the two C-terminal residues ($Ala_{41}Val_{42}$) on Aβ assembly and morphology in the presence of Cu^{2+} has implications for cytotoxicity and membrane disruption. Cu^{2+} loaded $A\beta_{(11-42)}$ generates some "curvy", short assemblies reminiscent of the protofibril and oligomer structures observed exclusively when substoichiometric Cu^{2+} is added to $A\beta_{(1-42)}$ fibres (24).

In conclusion, the N-terminally truncated form of Aβ constitutes relatively high levels in the CSF and plaques of Alzheimer's patients (11-13). Here we show $A\beta_{(11-40/42)}$ has marked amyloidogenicity and a femtomolar affinity for Cu^{2+}. The affinity of Cu^{2+} for Aβ has been a source of much attention, with much debate surrounding the ability of $A\beta_{(1-40/42)}$ to retain Cu^{2+} *in vivo* with a 50 pM affinity (35). The 34 femtomolar conditional affinity of $A\beta_{(11-40/42)}$ for Cu^{2+} is considerably tighter than extracellular competitors, such as serum albumin. We suggest the high abundance (19%) of $A\beta_{(11-40/42)}$ in plaques (12,13) must contribute to the high levels of Cu^{2+} reported in plaques (25,27,28). Furthermore a second N-terminally truncated form of Aβ, residues 4-40/42, is also found in plaques and typically makes up 6% of plaque load (12). This peptide also contains a histidine at the third position from the N-terminus and has recently been shown to bind Cu^{2+} with a sub-picomolar affinity (77). A further N-terminally truncated form, Aβ(3-40/42) is also found within plaques and is thought to constitute 2% of plaque load (12). Its Cu^{2+} binding properties have been carefully described (78). This complex does not have a histidine at the third position and forms a Cu^{2+} complex more similar to Aβ(1-40/42). Cu^{2+} within the plaques can convert $A\beta_{(1-42)}$ fibres into protofibrils/oligomers which suggests a mechanism to generate more toxic Aβ species

(24). Furthermore, the concentration of redox active Cu^{2+} within plaques can explain the high levels of methionine sulfoxide as well as di-tyrosine formation observed in Aβ plaques (27,79). The femtomolar affinity of $A\beta_{(11-40/42)}$ for Cu^{2+} has implications for chelation therapies targeting extracellular Cu^{2+}, and the mode of action of Clioquinol and its derivatives (32,34).

Acknowledgements: We want to express our gratitude to Harold Toms and Ray Burton-Smith for their assistance with NMR and EPR spectroscopy respectively. This research was funded by a Queen Mary University of London college studentship.

Conflict of interest: The authors declare that they have no conflicts of interest with the contents of this article.

Author Contributions: JDB performed experimental work, interpretation of data and preparation of the manuscript. JHV supervised planning and research, data interpretation and preparation of the manuscript.

REFERENCES

1. Prince, M., Jackson, J., Ferri, C. P., Sousa, R., Albanese, E., Ribeiro, W. S., and Honyashiki, M. (2009) Alzheimer's disease international world alzheimer report. *In International AsD (ed)*, pp. 1-96
2. Hardy, J. A., and Higgins, G. A. (1992) ALZHEIMERS-DISEASE - THE AMYLOID CASCADE HYPOTHESIS. *Science* **256**, 184-185
3. Kummer, M. P., and Heneka, M. T. (2014) Truncated and modified amyloid-beta species. *Alzheimers Res Ther* **6**, 28
4. Kang, J., Lemaire, H. G., Unterbeck, A., Salbaum, J. M., Masters, C. L., Grzeschik, K. H., Multhaup, G., Beyreuther, K., and Muller-Hill, B. (1987) The precursor of Alzheimer's disease amyloid A4 protein resembles a cell-surface receptor. *Nature* **325**, 733-736
5. Prelli, F., Castano, E., Glenner, G. G., and Frangione, B. (1988) Differences between vascular and plaque core amyloid in Alzheimer's disease. *J Neurochem* **51**, 648-651
6. Sevalle, J., Amoyel, A., Robert, P., Fournie-Zaluski, M. C., Roques, B., and Checler, F. (2009) Aminopeptidase A contributes to the N-terminal truncation of amyloid beta-peptide. *J Neurochem* **109**, 248-256
7. Mori, H., Takio, K., Ogawara, M., and Selkoe, D. J. (1992) Mass spectrometry of purified amyloid beta protein in Alzheimer's disease. *J Biol Chem* **267**, 17082-17086
8. Schilling, S., Lauber, T., Schaupp, M., Manhart, S., Scheel, E., Bohm, G., and Demuth, H. U. (2006) On the seeding and oligomerization of pGlu-amyloid peptides (in vitro). *Biochemistry* **45**, 12393-12399
9. Vassar, R., Bennett, B. D., Babu-Khan, S., Kahn, S., Mendiaz, E. A., Denis, P., Teplow, D. B., Ross, S., Amarante, P., Loeloff, R., Luo, Y., Fisher, S., Fuller, J., Edenson, S., Lile, J., Jarosinski, M. A., Biere, A. L., Curran, E., Burgess, T., Louis, J. C., Collins, F., Treanor, J., Rogers, G., and Citron, M. (1999) Beta-secretase cleavage of Alzheimer's amyloid precursor protein by the transmembrane aspartic protease BACE. *Science* **286**, 735-741
10. Huse, J. T., Liu, K. N., Pijak, D. S., Carlin, D., Lee, V. M. Y., and Doms, R. W. (2002) beta-secretase processing in the trans-Golgi network preferentially generates truncated amyloid species that accumulate in Alzheimer's disease brain. *Journal of Biological Chemistry* **277**, 16278-16284

11. Seubert, P., Vigo-Pelfrey, C., Esch, F., Lee, M., Dovey, H., Davis, D., Sinha, S., Schlossmacher, M., Whaley, J., Swindlehurst, C., and et al. (1992) Isolation and quantification of soluble Alzheimer's beta-peptide from biological fluids. *Nature* **359**, 325-327
12. Naslund, J., Schierhorn, A., Hellman, U., Lannfelt, L., Roses, A. D., Tjernberg, L. O., Silberring, J., Gandy, S. E., Winblad, B., Greengard, P., Nordstedt, C., and Terenius, L. (1994) RELATIVE ABUNDANCE OF ALZHEIMER A-BETA AMYLOID PEPTIDE VARIANTS IN ALZHEIMER-DISEASE AND NORMAL AGING. *Proceedings of the National Academy of Sciences of the United States of America* **91**, 8378-8382
13. Liu, K., Solano, I., Mann, D., Lemere, C., Mercken, M., Trojanowski, J. Q., and Lee, V. M. Y. (2006) Characterization of A beta 11-40/42 peptide deposition in Alzheimer's disease and young Down's syndrome brains: implication of N-terminally truncated A beta species in the pathogenesis of Alzheimer's disease. *Acta Neuropathologica* **112**, 163-174
14. Schilling, S., Hoffmann, T., Manhart, S., Hoffmann, M., and Demuth, H. U. (2004) Glutaminyl cyclases unfold glutamyl cyclase activity under mild acid conditions. *FEBS Lett* **563**, 191-196
15. Kuo, Y. M., Kokjohn, T. A., Beach, T. G., Sue, L. I., Brune, D., Lopez, J. C., Kalback, W. M., Abramowski, D., Sturchler-Pierrat, C., Staufenbiel, M., and Roher, A. E. (2001) Comparative analysis of amyloid-beta chemical structure and amyloid plaque morphology of transgenic mouse and Alzheimer's disease brains. *J Biol Chem* **276**, 12991-12998
16. Sullivan, C. P., Berg, E. A., Elliott-Bryant, R., Fishman, J. B., McKee, A. C., Morin, P. J., Shia, M. A., and Fine, R. E. (2011) Pyroglutamate-A beta 3 and 11 colocalize in amyloid plaques in Alzheimer's disease cerebral cortex with pyroglutamate-A beta 11 forming the central core. *Neuroscience Letters* **505**, 109-112
17. Sudoh, S., Kawamura, Y., Sato, S., Wang, R., Saido, T. C., Oyama, F., Sakaki, Y., Komano, H., and Yanagisawa, K. (1998) Presenilin 1 mutations linked to familial Alzheimer's disease increase the intracellular levels of amyloid beta-protein 1-42 and its N-terminally truncated variant(s) which are generated at distinct sites. *J Neurochem* **71**, 1535-1543
18. Pike, C. J., Overman, M. J., and Cotman, C. W. (1995) Amino-terminal deletions enhance aggregation of beta-amyloid peptides in vitro. *J Biol Chem* **270**, 23895-23898
19. Viles, J. H. (2012) Metal ions and amyloid fiber formation in neurodegenerative diseases. Copper, zinc and iron in Alzheimer's, Parkinson's and prion diseases. *Coord. Chem. Rev.* **256**, 2271-2284
20. Smith, D. P., Ciccotosto, G. D., Tew, D. J., Fodero-Tavoletti, M. T., Johanssen, T., Masters, C. L., Barnham, K. J., and Cappai, R. (2007) Concentration dependent Cu2+ induced aggregation and dityrosine formation of the Alzheimer's disease amyloid-beta peptide. *Biochemistry* **46**, 2881-2891
21. Tougu, V., Karafin, A., Zovo, K., Chung, R. S., Howells, C., West, A. K., and Palumaa, P. (2009) Zn(II)- and Cu(II)-induced non-fibrillar aggregates of amyloid-beta (1-42) peptide are transformed to amyloid fibrils, both spontaneously and under the influence of metal chelators. *J. Neurochem.* **110**, 1784-1795
22. Sarell, C. J., Wilkinson, S. R., and Viles, J. H. (2010) Substoichiometric levels of Cu2+ ions accelerate the kinetics of fiber formation and promote cell toxicity of amyloid-{beta} from Alzheimer disease. *J. Biol. Chem.* **285**, 41533-41540
23. Sharma, A. K., Pavlova, S. T., Kim, J., Kim, J., and Mirica, L. M. (2013) The effect of Cu(2+) and Zn(2+) on the Abeta42 peptide aggregation and cellular toxicity. *Metallomics* **5**, 1529-1536
24. Matheou, C. J., Younan, N. D., and Viles, J. H. (2015) Cu2+ accentuates distinct misfolding of Abeta(1-40) and Abeta(1-42) peptides, and potentiates membrane disruption. *Biochem J* **466**, 233-242

25. Lovell, M. A., Robertson, J. D., Teesdale, W. J., Campbell, J. L., and Markesbery, W. R. (1998) Copper, iron and zinc in Alzheimer's disease senile plaques. *J. Neurol. Sci.* **18**, 47-52
26. Cherny, R. A., Legg, J. T., McLean, C. A., Fairlie, D. P., Huang, X., Atwood, C. S., Beyreuther, K., Tanzi, R. E., Masters, C. L., and Bush, A. I. (1999) Aqueous dissolution of Alzheimer's disease Abeta amyloid deposits by biometal depletion. *J Biol Chem* **274**, 23223-23228
27. Dong, J., Atwood, C. S., Anderson, V. E., Siedlak, S. L., Smith, M. A., Perry, G., and Carey, P. R. (2003) Metal binding and oxidation of amyloid-beta within isolated senile plaque cores: Raman microscopic evidence. *Biochemistry* **42**, 2768-2773
28. Miller, L. M., Wang, Q., Telivala, T. P., Smith, R. J., Lanzirotti, A., and Miklossy, J. (2006) Synchrotron-based infrared and X-ray imaging shows focalized accumulation of Cu and Zn co-localized with beta-amyloid deposits in Alzheimer's disease. *J. Struct. Biol.* **155**, 30-37
29. Sparks, D. L., and Schreurs, B. G. (2003) Trace amounts of copper in water induce beta-amyloid plaques and learning deficits in a rabbit model of Alzheimer's disease. *Proc. Natl. Acad. Sci. U. S. A.* **100**, 11065-11069
30. Sanokawa-Akakura, R., Cao, W., Allan, K., Patel, K., Ganesh, A., Heiman, G., Burke, R., Kemp, F. W., Bogden, J. D., Camakaris, J., Birge, R. B., and Konsolaki, M. (2010) Control of Alzheimer's amyloid beta toxicity by the high molecular weight immunophilin FKBP52 and copper homeostasis in Drosophila. *Plos One* **5**, e8626
31. Singh, I., Sagare, A. P., Coma, M., Perlmutter, D., Gelein, R., Bell, R. D., Deane, R. J., Zhong, E., Parisi, M., Ciszewski, J., Kasper, R. T., and Deane, R. (2013) Low levels of copper disrupt brain amyloid-beta homeostasis by altering its production and clearance. *Proc Natl Acad Sci U S A* **110**, 14771-14776
32. Cherny, R. A., Atwood, C. S., Xilinas, M. E., Gray, D. N., Jones, W. D., McLean, C. A., Barnham, K. J., Volitakis, I., Fraser, F. W., Kim, Y., Huang, X., Goldstein, L. E., Moir, R. D., Lim, J. T., Beyreuther, K., Zheng, H., Tanzi, R. E., Masters, C. L., and Bush, A. I. (2001) Treatment with a copper-zinc chelator markedly and rapidly inhibits beta-amyloid accumulation in Alzheimer's disease transgenic mice. *Neuron* **30**, 665-676
33. Singh, S. K., Sinha, P., Mishra, L., and Srikrishna, S. (2013) Neuroprotective Role of a Novel Copper Chelator against Abeta 42 Induced Neurotoxicity. *Int. J. Alzheimers. Dis.* **2013**, 567128
34. Matlack, K. E., Tardiff, D. F., Narayan, P., Hamamichi, S., Caldwell, K. A., Caldwell, G. A., and Lindquist, S. (2014) Clioquinol promotes the degradation of metal-dependent amyloid-beta (Abeta) oligomers to restore endocytosis and ameliorate Abeta toxicity. *Proc Natl Acad Sci U S A* **111**, 4013-4018
35. Sarell, C. J., Syme, C. D., Rigby, S. E. J., and Viles, J. H. (2009) Copper(II) Binding to Amyloid-beta Fibrils of Alzheimer's Disease Reveals a Picomolar Affinity: Stoichiometry and Coordination Geometry Are Independent of A beta Oligomeric Form. *Biochemistry* **48**, 4388-4402
36. Jiang, D., Zhang, L., Grant, G. P., Dudzik, C. G., Chen, S., Patel, S., Hao, Y., Millhauser, G. L., and Zhou, F. (2013) The elevated copper binding strength of amyloid-beta aggregates allows the sequestration of copper from albumin: a pathway to accumulation of copper in senile plaques. *Biochemistry* **52**, 547-556
37. Alies, B., Renaglia, E., Rozga, M., Bal, W., Faller, P., and Hureau, C. (2013) Cu(II) affinity for the Alzheimer's peptide: tyrosine fluorescence studies revisited. *Anal Chem* **85**, 1501-1508
38. Hartter, D. E., and Barnea, A. (1988) Evidence for release of copper in the brain: depolarization-induced release of newly taken-up 67copper. *Synapse* **2**, 412-415
39. Kardos, J., Kovacs, I., Hajos, F., Kalman, M., and Simonyi, M. (1989) Nerve endings from rat brain tissue release copper upon depolarization. A possible role in regulating neuronal excitability. *Neurosci Lett* **103**, 139-144

40. Glennon, J. D., and Sarkar, B. (1982) Nickel(II) transport in human blood serum. Studies of nickel(II) binding to human albumin and to native-sequence peptide, and ternary-complex formation with L-histidine. *Biochem J* **203**, 15-23
41. Patel, S. U., Sadler, P. J., Tucker, A., and Viles, J. H. (1993) Direct-Detection of Albumin in Human Blood-Plasma by 1h Nmr-Spectroscopy - Complexation of Nickel2+. *Journal of the American Chemical Society* **115**, 9285-9286
42. Linder, M. C., Wooten, L., Cerveza, P., Cotton, S., Shulze, R., and Lomeli, N. (1998) Copper transport. *Am J Clin Nutr* **67**, 965S-971S
43. Rozga, M., Sokolowska, M., Protas, A. M., and Bal, W. (2007) Human serum albumin coordinates Cu(II) at its N-terminal binding site with 1 pM affinity. *J Biol Inorg Chem* **12**, 913-918
44. Bal, W., Christodoulou, J., Sadler, P. J., and Tucker, A. (1998) Multi-metal binding site of serum albumin. *J Inorg Biochem* **70**, 33-39
45. Lau, S. J., and Sarkar, B. (1971) Ternary coordination complex between human serum albumin, copper (II), and L-histidine. *J Biol Chem* **246**, 5938-5943
46. Masuoka, J., Hegenauer, J., Van Dyke, B. R., and Saltman, P. (1993) Intrinsic stoichiometric equilibrium constants for the binding of zinc(II) and copper(II) to the high affinity site of serum albumin. *J Biol Chem* **268**, 21533-21537
47. Fezoui, Y., Hartley, D. M., Harper, J. D., Khurana, R., Walsh, D. M., Condron, M. M., Selkoe, D. J., Lansbury, P. T., Jr., Fink, A. L., and Teplow, D. B. (2000) An improved method of preparing the amyloid beta-protein for fibrillogenesis and neurotoxicity experiments. *Amyloid* **7**, 166-178
48. Teplow, D. B. (2006) Preparation of amyloid beta-protein for structural and functional studies. *Methods Enzymol* **413**, 20-33
49. Kuipers, B. J. H., and Gruppen, H. (2007) Prediction of molar extinction coefficients of proteins and peptides using UV absorption of the constituent amino acids at 214 nm to enable quantitative reverse phase high-performance liquid chromatography-mass spectrometry analysis. *Journal of Agricultural and Food Chemistry* **55**, 5445-5451
50. Hatcher, L. Q., Hong, L., Bush, W. D., Carducci, T., and Simon, J. D. (2008) Quantification of the binding constant of copper(II) to the amyloid-beta peptide. *J Phys Chem B* **112**, 8160-8164
51. Dawson, R. M. C., Elliot, D. C., Elliot, W. H., and Jones, K. M. (1986) *Data for Biochemical Research*, Claredon Press, Oxford
52. Younan, N. D., and Viles, J. H. (2015) A comparison of three fluorophores (ThT, ANS, bis-ANS) for the detection of amyloid fibers and prefibrillar oligomeric assemblies. *Biochemistry*
53. Uversky, V. N., Li, J., and Fink, A. L. (2001) Metal-triggered structural transformations, aggregation, and fibrillation of human alpha-synuclein. A possible molecular NK between Parkinson's disease and heavy metal exposure. *J. Biol. Chem.* **276**, 44284-44296
54. Klewpatinond, M., Davies, P., Bowen, S., Brown, D. R., and Viles, J. H. (2008) Deconvoluting the Cu2+ binding modes of full-length prion protein. *J Biol Chem* **283**, 1870-1881
55. Stanyon, H. F., Patel, K., Begum, N., and Viles, J. H. (2014) Copper(II) sequentially loads onto the N-terminal amino group of the cellular prion protein before the individual octarepeats. *Biochemistry* **53**, 3934-3999
56. Tsangaris, J. M., and Martin, R. B. (1970) Visible circular dichroism of copper(II) complexes of amino acids and peptides. *J Am Chem Soc* **92**, 4255-4260
57. Klewpatinond, M., and Viles, J. H. (2007) Empirical rules for rationalising visible circular dichroism of Cu2+ and Ni2+ histidine complexes: applications to the prion protein. *FEBS Lett* **581**, 1430-1434
58. Stanyon, H. F., Cong, X., Chen, Y., Shahidullah, N., Rossetti, G., Dreyer, J., Papamokos, G., Carloni, P., and Viles, J. H. (2014) Developing predictive rules for coordination geometry from visible

circular dichroism of copper(II) and nickel(II) ions in histidine and amide main-chain complexes. *FEBS J* **281**, 3945-3954

59. Peisach, J., and Blumberg, W. E. (1974) STRUCTURAL IMPLICATIONS DERIVED FROM ANALYSIS OF ELECTRON-PARAMAGNETIC RESONANCE-SPECTRA OF NATURAL AND ARTIFICIAL COPPER PROTEINS. *Archives of Biochemistry and Biophysics* **165**, 691-708
60. Gala, L., Lawson, M., Jomova, K., Zelenicky, L., Congradyova, A., Mazur, M., and Valko, M. (2014) EPR spectroscopy of a clinically active (1:2) copper(II)-histidine complex used in the treatment of Menkes disease: a Fourier transform analysis of a fluid CW-EPR spectrum. *Molecules* **19**, 980-991
61. Lambert, M. P., Barlow, A. K., Chromy, B. A., Edwards, C., Freed, R., Liosatos, M., Morgan, T. E., Rozovsky, I., Trommer, B., Viola, K. L., Wals, P., Zhang, C., Finch, C. E., Krafft, G. A., and Klein, W. L. (1998) Diffusible, nonfibrillar ligands derived from Abeta1-42 are potent central nervous system neurotoxins. *Proc. Natl. Acad. Sci. U. S. A.* **95**, 6448-6453
62. Walsh, D. M., Klyubin, I., Fadeeva, J. V., Cullen, W. K., Anwyl, R., Wolfe, M. S., Rowan, M. J., and Selkoe, D. J. (2002) Naturally secreted oligomers of amyloid beta protein potently inhibit hippocampal long-term potentiation in vivo. *Nature* **416**, 535-539
63. Lesne, S., Koh, M. T., Kotilinek, L., Kayed, R., Glabe, C. G., Yang, A., Gallagher, M., and Ashe, K. H. (2006) A specific amyloid-beta protein assembly in the brain impairs memory. *Nature* **440**, 352-357
64. Yankner, B. A., and Lu, T. (2009) Amyloid beta-protein toxicity and the pathogenesis of Alzheimer disease. *J. Biol. Chem.* **284**, 4755-4759
65. Hortschansky, P., Schroeckh, V., Christopeit, T., Zandomeneghi, G., and Fandrich, M. (2005) The aggregation kinetics of Alzheimer's beta-amyloid peptide is controlled by stochastic nucleation. *Protein Sci* **14**, 1753-1759
66. Knowles, T. P., Waudby, C. A., Devlin, G. L., Cohen, S. I., Aguzzi, A., Vendruscolo, M., Terentjev, E. M., Welland, M. E., and Dobson, C. M. (2009) An analytical solution to the kinetics of breakable filament assembly. *Science* **326**, 1533-1537
67. Xue, W. F., Hellewell, A. L., Gosal, W. S., Homans, S. W., Hewitt, E. W., and Radford, S. E. (2009) Fibril fragmentation enhances amyloid cytotoxicity. *J Biol Chem* **284**, 34272-34282
68. Schutz, A. K., Vagt, T., Huber, M., Ovchinnikova, O. Y., Cadalbert, R., Wall, J., Guntert, P., Bockmann, A., Glockshuber, R., and Meier, B. H. (2015) Atomic-resolution three-dimensional structure of amyloid beta fibrils bearing the Osaka mutation. *Angew Chem Int Ed Engl* **54**, 331-335
69. Tycko, R. (2004) Progress towards a molecular-level structural understanding of amyloid fibrils. *Curr Opin Struct Biol* **14**, 96-103
70. Whittemore, N. A., Mishra, R., Kheterpal, I., Williams, A. D., Wetzel, R., and Serpersu, E. H. (2005) Hydrogen-deuterium (H/D) exchange mapping of Abeta 1-40 amyloid fibril secondary structure using nuclear magnetic resonance spectroscopy. *Biochemistry* **44**, 4434-4441
71. Olofsson, A., Lindhagen-Persson, M., Sauer-Eriksson, A. E., and Ohman, A. (2007) Amide solvent protection analysis demonstrates that amyloid-beta(1-40) and amyloid-beta(1-42) form different fibrillar structures under identical conditions. *Biochem J* **404**, 63-70
72. Strozyk, D., Launer, L. J., Adlard, P. A., Cherny, R. A., Tsatsanis, A., Volitakis, I., Blennow, K., Petrovitch, H., White, L. R., and Bush, A. I. (2009) Zinc and copper modulate Alzheimer Abeta levels in human cerebrospinal fluid. *Neurobiol Aging* **30**, 1069-1077
73. Karr, J. W., Akintoye, H., Kaupp, L. J., and Szalai, V. A. (2005) N-Terminal deletions modify the Cu2+ binding site in amyloid-beta. *Biochemistry*, 44:5478-5487

74. Karr, J. W., and Szalai, V. A. (2008) Cu(II) binding to monomeric, oligomeric, and fibrillar forms of the Alzheimer's disease amyloid-beta peptide. *Biochemistry* **47**, 5006-5016
75. Parthasarathy, S., Long, F., Miller, Y., Xiao, Y., McElheny, D., Thurber, K., Ma, B., Nussinov, R., and Ishii, Y. (2011) Molecular-level examination of Cu2+ binding structure for amyloid fibrils of 40-residue Alzheimer's beta by solid-state NMR spectroscopy. *J. Am. Chem. Soc.* **133**, 3390-3400
76. Gunderson, W. A., Hernandez-Guzman, J., Karr, J. W., Sun, L., Szalai, V. A., and Warncke, K. (2012) Local structure and global patterning of Cu2+ binding in fibrillar amyloid-beta [Abeta(1-40)] protein. *J. Am. Chem. Soc.* **134**, 18330-18337
77. Mital, M., Wezynfeld, N. E., Fraczyk, T., Wiloch, M. Z., Wawrzyniak, U. E., Bonna, A., Tumpach, C., Barnham, K. J., Haigh, C. L., Bal, W., and Drew, S. C. (2015) A Functional Role for Abeta in Metal Homeostasis? N-Truncation and High-Affinity Copper Binding. *Angew Chem Int Ed Engl*
78. Alies, B., Bijani, C., Sayen, S., Guillon, E., Faller, P., and Hureau, C. (2012) Copper coordination to native N-terminally modified versus full-length amyloid-beta: second-sphere effects determine the species present at physiological pH. *Inorg Chem* **51**, 12988-13000
79. Al-Hilaly, Y. K., Williams, T. L., Stewart-Parker, M., Ford, L., Skaria, E., Cole, M., Bucher, W. G., Morris, K. L., Sada, A. A., Thorpe, J. R., and Serpell, L. C. (2013) A central role for dityrosine crosslinking of Amyloid-beta in Alzheimer's disease. *Acta neuropathologica communications* **1**, 83

FIGURE LEGENDS

FIGURE 1. β- and β′- secretase processing of amyloid precursor protein (APP). The β′ activity of the beta-site amyloid precursor protein cleaving enzyme 1 (BACE-1) N-terminally truncates Aβ before Glu_{11}. γ-secretase cleaves the C-terminus most commonly at position 40 or 42, within the lipid bilayer. The α-secretase produces P3 which starts at Lys17. The percentages of typical Aβ plaque load are also indicated; 19% for $Aβ_{(11-40/42)}$.

FIGURE 2. $Aβ_{(11-40)}$ and $Aβ_{(11-42)}$ form amyloid rods. ThT Fluorescence follows the fibre growth of $Aβ_{(11-40)}$ (blue), $Aβ_{(11-42)}$ (green) and $Aβ_{(1-40)}$ (red) (a). Representative TEM images of $Aβ_{(11-40)}$ (b), $Aβ_{(1-40)}$ (c) and $Aβ_{(11-42)}$ (e,f) negatively stained with phosphotungstenic acid, the scale bar is 200 nm. Fibre lengths were measured for $Aβ_{(11-40)}$ (blue) and $Aβ_{(1-40)}$ (red) and their percentage frequency is shown in (d). N-terminally truncated Aβ forms fibres more rapidly than full length Aβ and produces short stacked amyloid rods, mild intermittent agitation for all conditions, 10 μM peptide, 10 μM ThT, 30 mM HEPES, 160 mM NaCl at pH 7.4.

FIGURE 3. Quiescently grown fibres of $Aβ_{(11-40)}$ (a) and $Aβ_{(11-42)}$ (b). Representative TEM images after 20 days incubation at room temperature with no agitation, 10 μM peptide, pH 7.4, 160 mM NaCl, 30 mM HEPES. Under quiescent growth conditions much longer fibres are observed. Scale bars are 200 nm.

FIGURE 4. Cu^{2+} visible CD of $Aβ_{(11-40)}$ and $Aβ_{(11-15)}$. Overlaid spectra of $Aβ_{(11-40)}$ (red), $Aβ_{(11-15)}$ (green) (a). Comparison of N-terminally truncated $Aβ_{(11-40)}$ (red) and $Aβ_{(11-15)}$ (green) with albumin (orange) and its peptide mimics AAH (blue) and DAH (purple) (b). Cu^{2+} titration with $Aβ_{(11-15)}$ shows signal saturation at 1:1 stoichiometry (spectra as inset) The dotted lines are straight line fits to the initial data points and the points in which saturation is apparent. (c). pH dependence of the EVHHQ Cu^{2+} complex, pKa = 4.7 (spectra are shown as inset) (d). 100 μM Peptides, pH 7.4.

FIGURE 5. Comparison of Cu^{2+}-EPR spectra of Cu^{2+} $Aβ_{(11-15)}$ with Cu^{2+} DAH (The N-terminal residues of albumin AspAlaHis). EPR shows highly similar spectra, indicating the same 4N square-planar coordination geometry (a). 100 μM Peptides, 90 μM $CuCl_2$ at pH 7.4 in 50 mM 60% HEPES/40% phosphate buffer. Proposed 4N square planar coordination geometry of Cu^{2+} $Aβ_{(11-40)}$. Axial coordination from the imidazole nitrogen of His_{14} is also probable (b).

FIGURE 6. Cu^{2+} binds to $Aβ_{(11-40)}$ fibres. A comparison of vis-CD spectra of Cu^{2+} loaded monomer (red) and fibres (blue) of $Aβ_{(11-40)}$. The inset shows $Aβ_{(11-40)}$ fibres loading Cu^{2+} with approximate 1:1 stoichiometry (0.7 : 1). Preformed $Aβ_{(11-40)}$ fibres (70 μM) were generated prior to Cu^{2+} titration, pH 7.4. $Aβ_{(11-40)}$ fibres can accommodate Cu^{2+} binding in the same manner as the monomeric form, with similar CD bands and intensities.

FIGURE 7. Cu^{2+} affinity for $Aβ_{(11-40)}$ competitive titrations. Visible CD of $Aβ_{(11-15)}$ using L-histidine (a) and glycine competitors (b). Cu^{2+} $Aβ_{(11-40)}$ complex titrated with glycine (c). The dotted line shows the concentration of competitor needed to remove half the Cu^{2+} from the Aβ peptides. Inserts show vis-CD spectra with increasing concentrations of competitor. All experiments were carried out at pH 7.4 with $Aβ_{(11-15)}$ at 100 μM. $Aβ_{(11-40)}$ is at 72 μM.

FIGURE 8. Influence of Cu^{2+} on $A\beta_{(11-40)}$ and $A\beta_{(11-42)}$ fibre growth. ThT Fluorescence of $A\beta_{(11-40)}$ and $A\beta_{(11-42)}$ fibre growth with different molar equivalencies of $Cu^{2+,}$ (a) and (d) respectively. TEM images of fibres produced with the following Cu^{2+} equivalencies: $A\beta_{(11-40)}$ 0.1 (b) 0.4 (c). $A\beta_{(11-42)}$ 0.1 (e) 0.4 (f). All scale bars are 50 nm.

FIGURE 9. Reversibility of Cu^{2+} influence on $A\beta_{(11-40)}$ fibres**.** The effect of 0.4 molar equivalents Cu^{2+} on pre-formed $A\beta_{(11-40)}$ fibres and removal of Cu^{2+} from Cu^{2+} $A\beta_{(11-40)}$ fibres. ThT Fluorescence of $A\beta_{(11-40)}$ fibre growth with subsequent addition of 0.4 molar equivalents Cu^{2+} at 235 hrs. Also showing fibre growth of $A\beta_{(11-40)}$ in the presence of Cu^{2+} with later addition of 0.4 molar equivalents of EDTA (a). ThT fluorescence kinetics traces are an average from n = 6, error bars are SEM. TEM images of the fibres produced with Cu^{2+} added to preformed fibres (b) and Cu^{2+} $A\beta_{(11-40)}$ fibres with subsequent EDTA addition (c). Scale bars are 200 nm.

TABLES

TABLE 1. Femtomolar conditional dissociation constants (K_d) at pH 7.4 shown for $A\beta_{(11-40)}$ and its peptide models $A\beta_{(11-15)}$ and $A\beta_{(11-15)}$ $His_{14}Ala$.

Peptide	Glycine	Histidine	Mean
$A\beta_{(11-15)}$	27 ± 3 and 24 ± 3	50 ± 16 and 34 ± 2	34 ± 5 fM
$A\beta_{(11-40)}$	10 ± 3	–	10 ± 3 fM
$A\beta_{(11-15)}$ $H_{14}A$	186 ± 27	87 ± 9	136 ± 23 fM

FIGURE 1

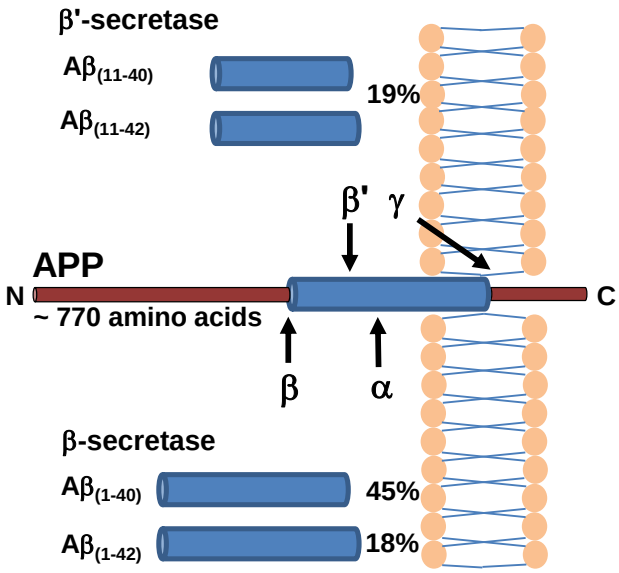
β'-secretase
Aβ(11-40)
Aβ(11-42)
19%
β'
γ
APP
N
C
~ 770 amino acids
β
α
β-secretase
Aβ(1-40)
Aβ(1-42)
45%
18%

FIGURE 2

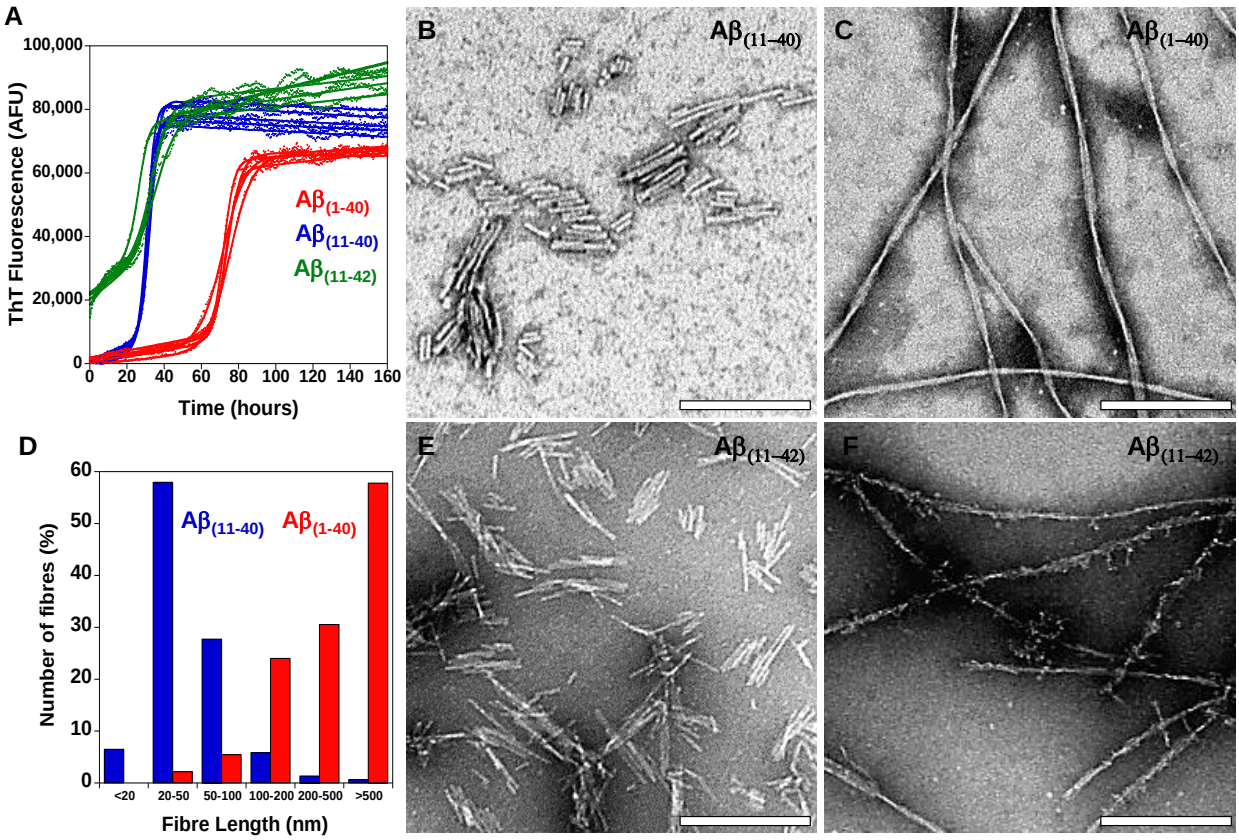
A
100,000
80,000
60,000
40,000
20,000
0
ThT Fluorescence (AFU)
0 20 40 60 80 100 120 140 160
Time (hours)
Aβ(1-40)
Aβ(11-40)
Aβ(11-42)
B
Aβ(11–40)
C
Aβ(1–40)
D
60
50
40
30
20
10
0
Number of fibres (%)
Aβ(11-40)
Aβ(1-40)
<20
20-50
50-100
100-200
200-500
>500
Fibre Length (nm)
E
Aβ(11–42)
F
Aβ(11–42)

FIGURE 3

a) Aβ$_{(11-40)}$

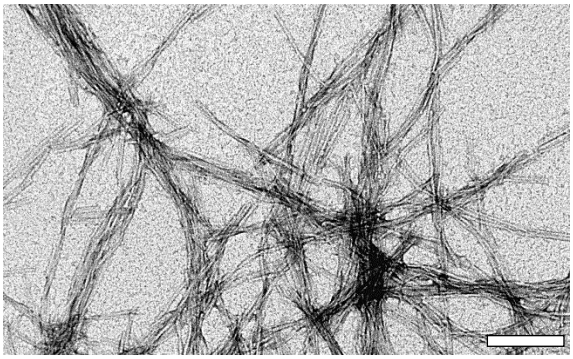

b) Aβ$_{(11-42)}$

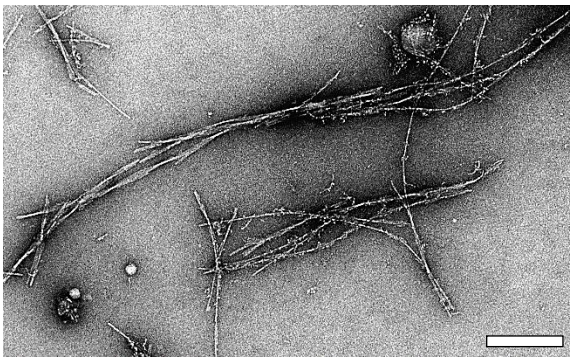

FIGURE 4

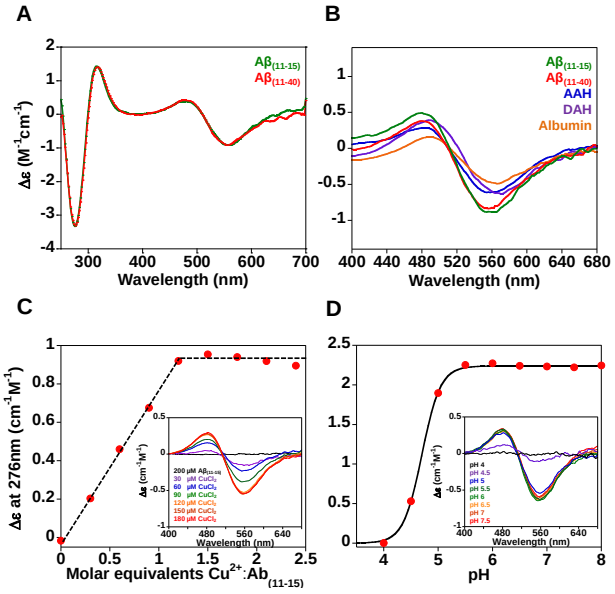
A
B
C
D
Aβ(11-15)
Aβ(11-40)
AAH
DAH
Albumin
Δε (M-1cm-1)
Wavelength (nm)
Δε at 276nm (cm-1M-1)
Molar equivalents Cu2+:Ab(11-15)
pH

FIGURE 5

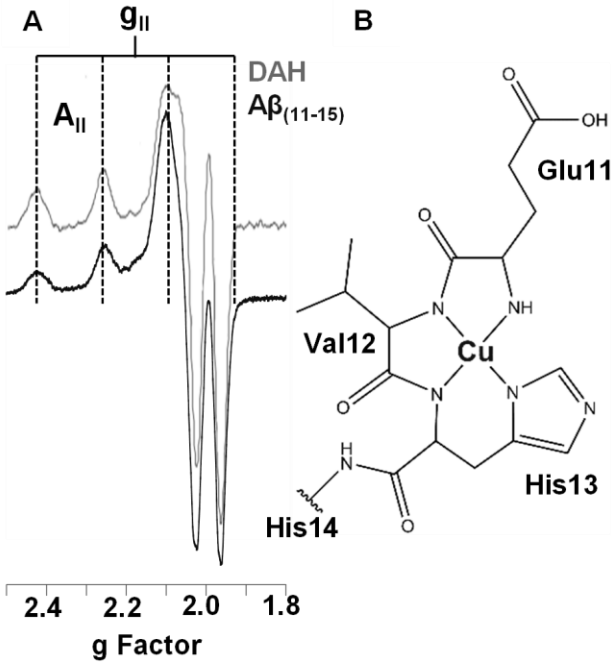
A
g_{II}
A_{II}
DAH
$A\beta_{(11-15)}$
2.4
2.2
2.0
1.8
g Factor
B
O
OH
Glu11
O
N
NH
Val12
Cu
O
N
N
N
H
N
His13
His14
O

FIGURE 6

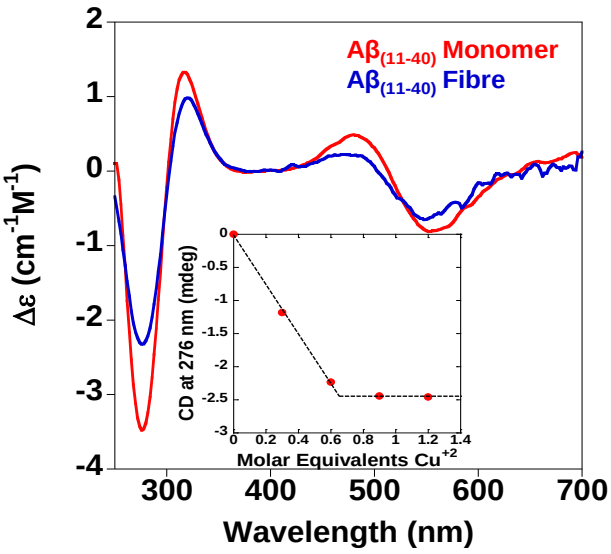
Aβ(11-40) Monomer
Aβ(11-40) Fibre
Δε (cm-1M-1)
Wavelength (nm)
CD at 276 nm (mdeg)
Molar Equivalents Cu+2

FIGURE 7

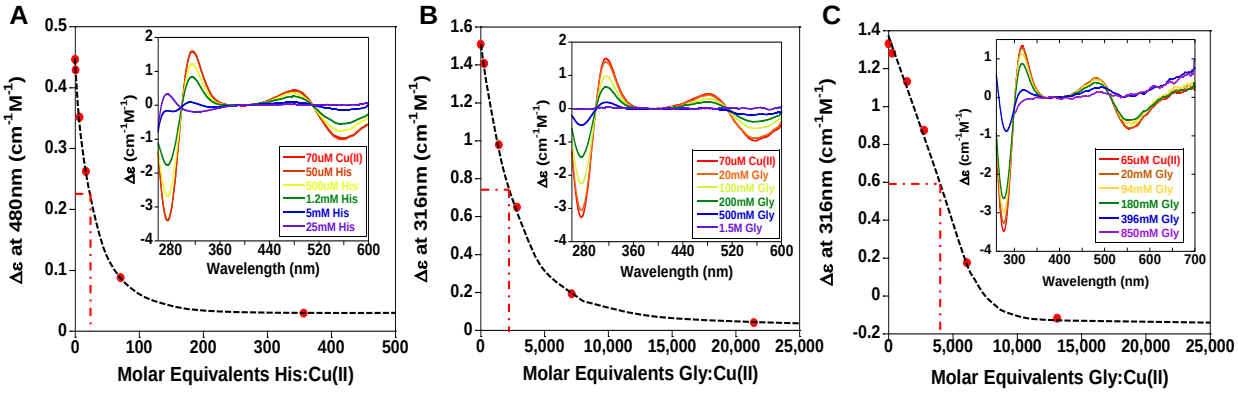
A
Δε at 480nm (cm-1M-1)
Molar Equivalents His:Cu(II)
Δε (cm-1M-1)
Wavelength (nm)
70uM Cu(II)
50uM His
500uM His
1.2mM His
5mM His
25mM His
B
Δε at 316nm (cm-1M-1)
Molar Equivalents Gly:Cu(II)
Δε (cm-1M-1)
Wavelength (nm)
70uM Cu(II)
20mM Gly
100mM Gly
200mM Gly
500mM Gly
1.5M Gly
C
Δε at 316nm (cm-1M-1)
Molar Equivalents Gly:Cu(II)
Δε (cm-1M-1)
Wavelength (nm)
65uM Cu(II)
20mM Gly
94mM Gly
180mM Gly
396mM Gly
850mM Gly

FIGURE 8

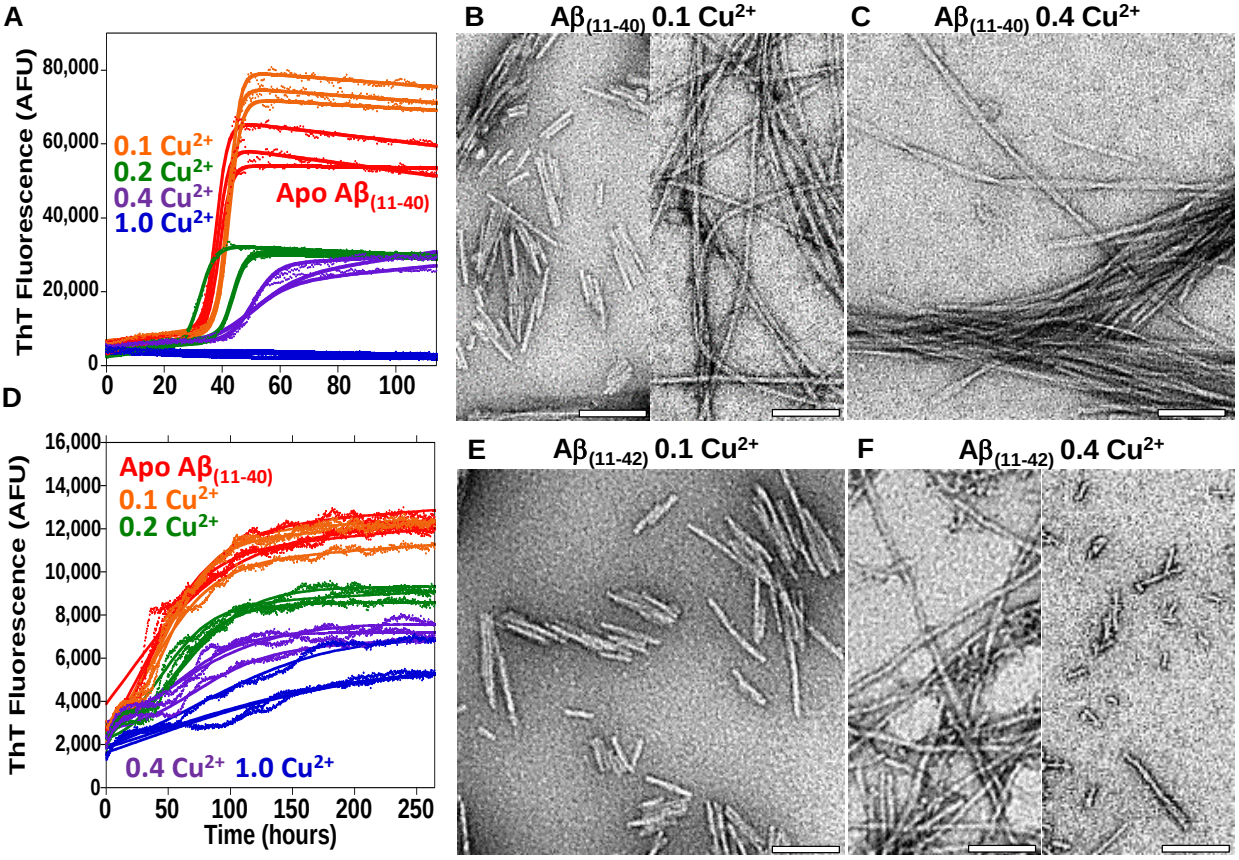
A
ThT Fluorescence (AFU)
80,000
60,000
40,000
20,000
0
0 20 40 60 80 100
0.1 Cu2+
0.2 Cu2+
0.4 Cu2+
1.0 Cu2+
Apo Aβ(11-40)
B
Aβ(11-40) 0.1 Cu2+
C
Aβ(11-40) 0.4 Cu2+
D
ThT Fluorescence (AFU)
16,000
14,000
12,000
10,000
8,000
6,000
4,000
2,000
0
0 50 100 150 200 250
Time (hours)
Apo Aβ(11-40)
0.1 Cu2+
0.2 Cu2+
0.4 Cu2+ 1.0 Cu2+
E
Aβ(11-42) 0.1 Cu2+
F
Aβ(11-42) 0.4 Cu2+

FIGURE 9

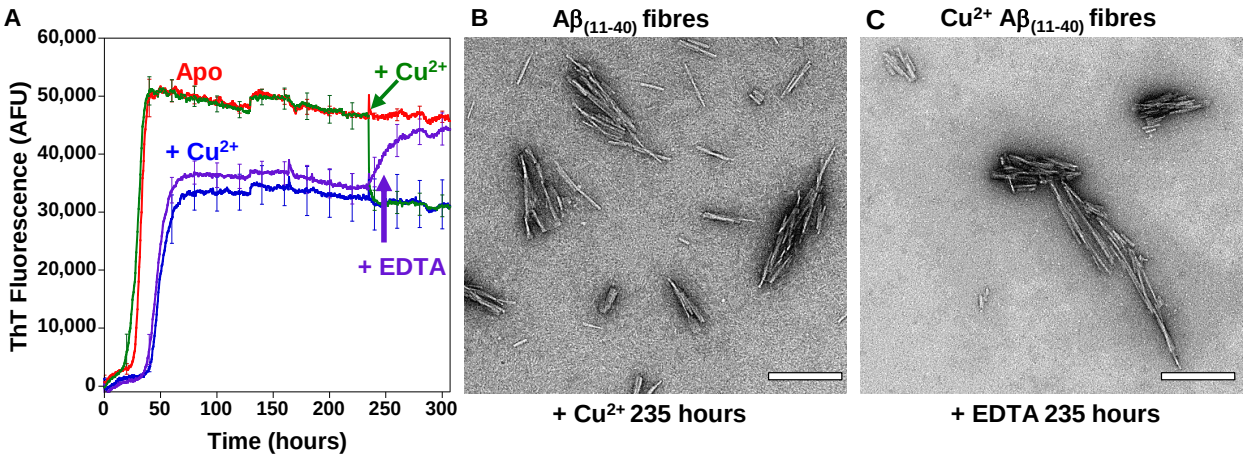
A
ThT Fluorescence (AFU)
60,000
50,000
40,000
30,000
20,000
10,000
0
0
50
100
150
200
250
300
Time (hours)
Apo
+ Cu2+
+ Cu2+
+ EDTA
B
Aβ(11-40) fibres
+ Cu2+ 235 hours
C
Cu2+ Aβ(11-40) fibres
+ EDTA 235 hours